Ablation Processes for HfC-Coated 2.5D Needle-Punched Composites Used for Aerospace Engines Under Hypersonic Flight Conditions

ZHANG Ziyi[1,2], *SHI Zhenyu*[3*], *NI Jing*[4], *WANG Jilai*[1,2], *ZHANG Chengpeng*[1,2]

1. Key Laboratory of High Efficiency and Clean Mechanical Manufacture (Ministry of Education), Shandong University, Jinan 250061, P. R. China;
2. School of Mechanical Engineering, Shandong University, Jinan 250061, P. R. China;
3. State Key Laboratory of Reliability and Intelligence of Electrical Equipment, School of Mechanical Engineering, Hebei University of Technology, Tianjin 300130, P. R. China;
4. School of Mechanical Engineering, Hangzhou Dianzi University, Hangzhou 310012, P. R. China

(Received 25 June 2024; revised 6 August 2024; accepted 28 September 2024)

Abstract: The working environment of aerospace engines is extremely harsh with temperature exceeding 1 700 ℃ and accompanied by thermal coupling effects. In this condition, the materials employed in hypersonic aircraft undergo ablation issues, which can cause catastrophic accidents. Due to the excellent high-temperature stability and ablation resistance, HfC exhibits outstanding thermal expansion coefficient matching that of C/SiC composites. 2.5D needle-punched C/SiC composites coated with HfC are prepared using a plasma spraying process, and a high-enthalpy arc-heated wind tunnel is employed to simulate the re-entry environment of aircraft at 8 Mach and an altitude of 32 km. The plasma-sprayed HfC-coated 2.5D needle-punched C/SiC composites are subjected to long-term dynamic testing, and their properties are investigated. Specifically, after the thermal assessment ablation experiment, the composite retains its overall structure and profile; the total mass ablation rate is 0.074 45 g/s, the average linear ablation rate in the thickness direction is −0.067 5 μm/s, and the average linear ablation rate in the length direction is 13.907 μm/s. Results verify that plasma-sprayed HfC coating exhibits excellent anti-oxidation and ablation resistance properties. Besides, the microstructure and ablation mechanism of the C/SiC composites are studied. It is believed that this work will offer guideline for the development of thermal protection materials and the assessment of structural thermal performance.

Key words: 2.5D needle-punched C/SiC composites; ablation mechanism; arc-heated wind tunnel experiment; high enthalpy flow

CLC number: TB332 **Document code:** A **Article ID:** 1005-1120(2024)05-0645-11

0 Introduction

Hypersonic vehicles fly at speeds exceeding 5 Mach (6 173 km/h)[1], which possesses unique physical characteristics, such as high speed, good penetration strength, and good concealment. They embolden the role of modern military, space technology, and scientific and technological progress[2]. Being a part of national security, the associated scientific and technological challenges in hypersonic aircraft boost research at the international level including the academic and engineering communities. During flight, the re-entry phase of a hypersonic vehicle is a critical stage, which undergoes extreme aerodynamic and thermal conditions. Hence, the development of an efficient thermal protection system (TPS) becomes crucial[3-4].

During the past decade, C/SiC composites

*Corresponding author, E-mail address: zyshi@hebut.edu.cn.

How to cite this article: ZHANG Ziyi, SHI Zhenyu, NI Jing, et al. Ablation processes for HfC-coated 2.5D needle-punched composites used for aerospace engines under hypersonic flight conditions[J]. Transactions of Nanjing University of Aeronautics and Astronautics, 2024, 41(5): 645-655.

http://dx.doi.org/10.16356/j.1005-1120.2024.05.009

have resisted oxidation better than C/C composites, and have exhibited high specific strength, large specific modulus, ablation resistance, and high-temperature resistance[5-8]. Therefore, C/SiC composites have numerous applications in aerospace[9-11], particularly in thermal protection systems like heat shields, wing leading edges, nose cones, and flaps of aircraft[12-14]. The development of hypersonic aircraft requires robust materials for thermal protection systems, while the long-term application temperature of C/SiC composites is less than 1 650 ℃[15], and severe ablation will occur at higher temperatures. The re-entry vehicle undergoes significant heat flow in extremely high-temperature and high-pressure environments. Therefore, it is crucial to improve the microstructure and composition of C/SiC composites to optimize their performance in these conditions, particularly in terms of high anti-oxidant capacity and ablation resistance. Previous studies[16-20] have demonstrated the effectiveness of applying a coating of ultra-high temperature materials on the surface. This method greatly improves the stability of C/SiC composite materials at high temperatures. The HfC coating can enhance hardness, melting point, and stability. Additionally, the melting point of HfO_2 is higher than that of ZrO_2[21], making HfC the best fit material for anti-oxidation ablation coating. Among reported coating methods, vacuum plasma spray technique endows a facile and broad-area covering approach for preparing coatings on C/SiC composites[21-22]. It enables high deposition efficiency and strong coating bonding[23-26]. Yoo et al.[27] reported HfC-coated composites using a SiC buffer layer via vacuum plasma spray process, and the buffer layer protected the internal carbon fibers. In light of this, the objective of this study is to enhance the ablation resistance of C/SiC composites by spraying a HfC coating on its surface using a plasma spraying process.

High-speed airflow erosion can accelerate the degradation of composites sustaining ultra-high temperatures. Currently, the impact of airflow ablation is measured through dynamic gas, simulating the material ablation performance. The arc-heated wind tunnel enables ideal conditions for simulating the re-entry of aircraft into the atmospheric environment on the ground. It is adopted globally to investigate the ablation performance during re-entry process. In contrast to oxyacetylene and other tests, the composition of the aerodynamic and thermal environment in the arc-heated wind tunnel allows for precise control of experimental conditions: airflow speed, pressure, and temperature[28]. It facilitates the least cost of replicating the actual aircraft flight environment. Considering the heat-proof design of the tunnel, the outcomes can reflect the real ablation effect more accurately. Kong et al.[29] simulated the heat transfer and expansion phenomena of coatings in C/SiC composites within arc-heated wind tunnels. Li et al.[28] investigated the evolution mechanism of the voids in C/SiC composites through arc-heated wind tunnel tests. Thus, it has a great advantage to assess the ablation performance by utilizing an arc-heated wind tunnel.

In this study, HfC coating is deposited on the surface of C/SiC composites using a plasma spray coating process. The high-enthalpy supersonic airflow test is conducted on the leading edge made from HfC-coated C/SiC composites. The arc-heated wind tunnel is utilized to simulate the actual aerodynamic heating conditions experienced by aircraft during atmospheric re-entry, resulting in accurate enthalpy, heat flow, and pressure. The experiment simulates a flight at a speed of 8 Mach and an altitude of 32 km. This work investigates the thermal performance and ablation behavior of C/SiC composites in a simulated environment.

1 Experiment

1.1 Materials

2.5-dimensional (2.5D) needled carbon fiber preform is prepared through chemical vapor infiltration technique. Domestic T300 carbon fibers of grade 12 000 is used, and carbon fibers are stacked alternately along 0° and 90° (unidirectional) with a chopped fiber tire mesh layer, forming the needle-punched fiber bundles with tire mesh layer, that is, a 2.5D needle-punched structure. The reactive melt infiltration process prepares SiC matrix on the pre-

form, resulting in C/SiC composites with a density of 2.2 g/cm^3. Then it is processed into a V-shaped passivation leading edge sample. The leading edge is designed with a smaller radius of curvature, which can reduce the aerodynamic heat (generated during re-entry of sharp structural parts). It is designed to effectively disperse the heat and guide heat, thereby simplifying the process and reducing the cost. A dense layer of HfC, with a thickness of 30 μm, is coated by plasma spraying process. The process parameters for the plasma-sprayed HfC coating are shown in Table 1.

Table 1 Process parameters of plasma sprayed HfC coating

Current/A	Primary gas flow rate/(L•min^{-1})	Secondary gas flow rate /(L•min^{-1})	Nozzle diameter/mm	Feed rate/(g•min^{-1})	Spray distance/mm
350	75	5	5.5	30	100

1.2 Ablation test

The thermal assessment test of the sample is conducted in an arc-heated wind tunnel. Fig.1 shows the arc-heated wind tunnel equipment system diagram.

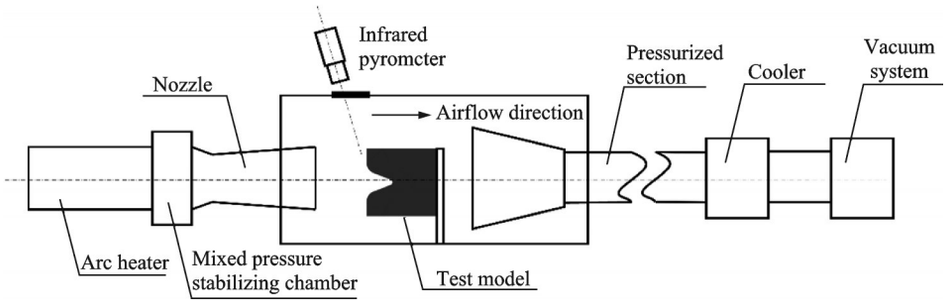

Fig.1 Diagram of arc-heated wind tunnel test equipment system

The macroscopic morphology of the leading edge sample is shown in Fig.2. The sample is vertically installed in the test fixture (along the airflow direction), as illustrated in Fig.2. An installed non-contact infrared thermometer (through a quartz glass observation window) measures the surface temperature of the leading edge regions: WT1, WT2 and WT3.

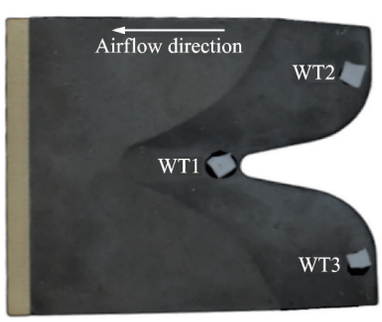

Fig.2 Macroscopic morphology of the leading edge sample

The detailed experimental parameters are listed in Table 2. States A, B, and C simulate the phase of climb, acceleration, and thermal environment during the cruise at 8 Mach and flight height of 32 km, respectively.

Table 2 Parameters of test conditions

State	Cold-wall heat flux/(MW•m^{-2})	Enthalpy value/(kJ•kg^{-1})	Pressure/kPa	Time/s
A	0.5	800	60	70
B	4.5	2 200	80	25
C	8	4 500	150	135

The corresponding curves depicting the temperature rise and test time of the test sample are illustrated in Fig.3.

The mass ablation rate (R_m) is calculated as follows

$$R_m = \frac{m_0 - m_1}{t} \tag{1}$$

where m_0 and m_1 represent the mass before and after ablation, respectively; t is the ablation time.

To assess the brittleness and susceptibility of the surface oxide layer to detachment, the thickness of the unaffected sample is measured. The linear ablation rate (R_l) of the sample is determined by measuring the size of the leading edge sample before and

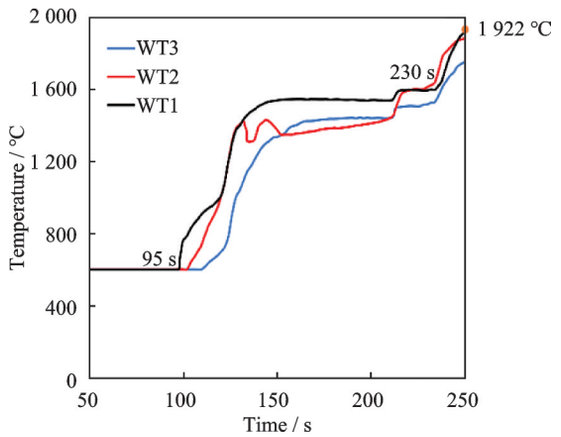

Fig.3 Surface temperature responses of sample in high-enthalpy flows

after ablation at multiple positions in the thickness direction using the three-coordinate method, and the results are averaged. R_l can be calculated by

$$R_l = \frac{1}{n}\sum_{i=1}^{n}(L_{i0} - L_{i1})/t \tag{2}$$

where L_{i0} and L_{i1} are the thickness at different positions before and after ablation, respectively.

1.3 Characterization

The microstructure and morphology of samples are characterized by scanning electron microscope (SEM, ZEISS GEMINI 300, Germany). The elemental composition analysis is collected by energy dispersion spectroscopy (EDS, OXFORD Ultim Max 40, UK). Phase analysis is performed by X-ray diffraction (XRD, ESCALAB Xi+, USA) equipped with Cu-Kα radiation. The variation in size (before and after ablation) is measured by three coordinate measuring machine (3D CMM). A two-color infrared pyrometer (Marathon MR1SC, Raytek, USA) is utilized to record the surface temperature of the sample.

2 Results and Discussion

2.1 Macroscopic ablation morphology

Fig.4(a) shows SEM analysis of C/SiC composites, revealing mainly C and Si phases. C phase consists of carbon fiber and pyrolytic carbon, as depicted in Fig.4(b). The key distinction lies in the variation in material structure. Si phase involves SiC and residual Si, as illustrated in Fig.4(c), which is primarily distributed among the short fiber web layer, the weftless cloth layer, and the needle-punched fiber bundle.

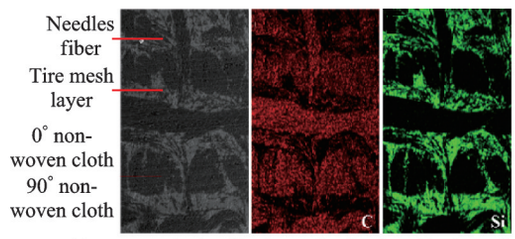

Fig.4 Microstructure and element distribution analysis diagram of C/SiC composites

Figs.5(a, b) show the macro morphologies of the sample after the arc-heated wind tunnel test. Compared with the morphology of the pre-ablation sample shown in Fig.2, it is found that the overall structure of the sample is intact, while the coating at the leading edge is torn out. There is no damage to the main structure of the leading edge. The front of the leading edge exhibits a thick deposition layer, while the back end possesses a loose and uneven deposition layer (Fig.5(c)). The area near the bottom of V-shaped is devoid of the deposition layer, exposing SiC matrix and carbon fiber. The tail end shows only surface ablation, the coating is blown off and the surface is nearly complete. Additionally, noticeable molten materials are observed on the front surface, and distinct flow traces can be seen at the front end of the back. From Fig.5(d), the surface of composite experiences melting, resulting in the forma-

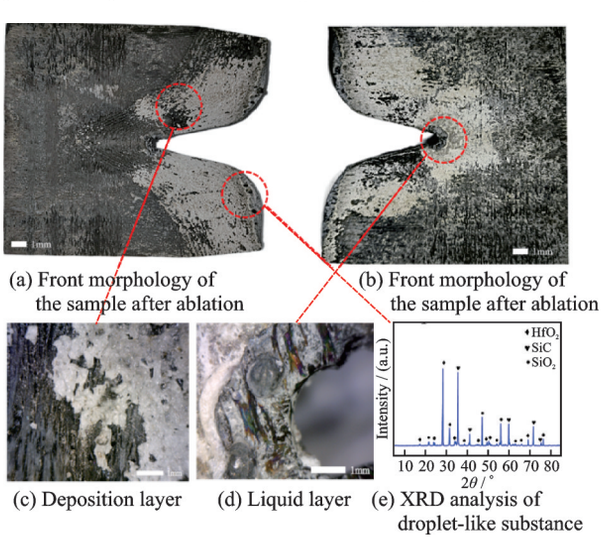

Fig.5 Morphology of the sample after ablation

tion of a liquid layer. This liquid layer flows and then evaporates along the surface due to aerodynamic shear. Consistent with the findings of Tang et al.[30], the thermal ablation process leads to the merging of liquid droplets and their presence in the form of a liquid film, which is more pronounced due to high ablation rate of liquid SiO_2. Fig.5(e) illustrates the presence of droplet-like substances on the surface. The melting point of SiC matrix is 2 380 ℃, and its sublimation temperature is 2 700 ℃. XRD analysis reveals that the droplet primarily consists of SiO_2 and SiC phases. The formation of liquid oxides accelerates the stagnation of composites[31], as liquid oxides disappear from the surface due to the dynamic pressure during arc-wind tunnel testing.

The temperature distribution in different regions of the leading edge is significantly asymmetric due to the large gradient of heat flux at the surface and the presence of asymmetric ablation. High surface heat flux and low thermal conductivity of composites cause a substantial temperature gradient along the radial direction. As shown in Fig.3, the highest temperature of the sample is observed to be 1 922 ℃ at the stagnation point WT1. Table 3 shows the measurement data of the mass and size of the sample before and after ablation. Calculated through Eqs.(1, 2), the overall mass ablation rate is 0.074 45 g/s, the average linear ablation rate in the thickness direction is −0.067 5 μm/s, and the average linear ablation rate in the length direction is 13.907 μm/s. The stagnation point WT2 in the central symmetric region exhibits the highest temperature, accompanied by high incoming flow pressure and heat flux, leading to the highest linear ablation rate and the most severe ablation—An ablation retreat of 7.05 mm.

Table 3 Mass and size data of sample before and after ablation

State	Mass/g	Thickness/mm				Length/mm		
		S_1	S_2	S_3	S_4	L_1	L_2	L_3
Initial	390.94	16.19	16.18	16.13	16.21	130.35	78.25	130.25
Post-ablation	374.04	16.16	16.26	16.12	16.23	129.39	71.20	128.79

Within the arc-heated wind tunnel environment, the combination of high temperature, high pressure, and high-speed flow makes the boundary layer thin, which increases the convective heat transfer and mass transfer processes of the gas on the surface[32]. This causes severe thermochemical corrosion of the material. Furthermore, the aerodynamic shearing further enhances the mechanical erosion of the material. Consequently, the material in the front end area undergoes severe ablation, causing the highest mass loss.

2.2 Microscopic ablation morphology

The oxidation resistance and ablation resistance of ceramic matrix composites are associated with the composition and microstructure of the surface oxide layer. So, the microscopic ablation morphology is examined at the stagnation point, which opens up the impact of temperature at the stagnation point.

The microstructure of the white deposition layer near the stagnation points of WT2 and WT3 is analyzed in Fig.6. From Fig.6(a), a dense structure covers the surface of the sample. The XRD spectrum analysis (Fig.6(c)) confirms that the white deposited layer consists of HfO_2 and SiO_2 phases (HfO_2 as the main component). SEM (Fig.6(b)) and XRD analysis (Fig.6(d)) of the inner layer of

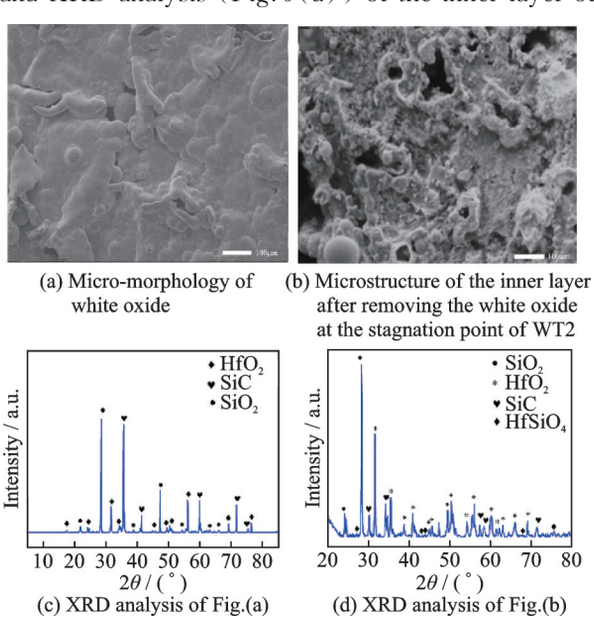

Fig.6 Microstructure of the white deposition layer near stagnation points of WT2 and WT3

the stagnation point reveal that the content of SiO_2 phase is higher than that of HfO_2. The inner layer exhibits a small amount of $HfSiO_4$ phase. As the temperature and heat flux density increase during the ablation process of HfC-coated C/SiC composites, the outer HfC coating is oxidized first. Due to airflow erosion, the oxide cannot form a stable anti-oxidation layer, leading to numerous oxygen lattice vacancies in the generated HfO_2. The HfO_2 oxide film is loosely bonded, allowing rapid diffusion of oxygen and passive oxidation of SiC matrix to generate SiO_2 in the exposed internal C/SiC composites. Both sides of the sample show minimal variation in size compared to the ablation retreat amount in the central area. Thus, HfO_2-SiO_2 oxide film slows down the diffusion of oxygen, and the oxidation resistance is ensured by the synergistic effect of the outer oxide layer and the inner dense layer, thereby reducing the amount of ablation.

Fig.7 shows the different morphologies of the inner surface after the removal of the white deposition layer at WT2. The morphology at low power lens of the surface is depicted in Fig.7(a). Fig.7(b) illustrates a favorable bonding state of the carbon fiber with PyC interface and SiC matrix. Fig.7(c) shows the micro-morphology of grooves and pores on the inner surface. According to the EDS analysis (Fig.7(d)), the carbon fiber has undergone severe ablation, and the exposed carbon fiber is wrapped up. The surface of the carbon fiber exhibits spherical SiO_2 particles (Figs. 7(e, f)), which are formed through the solidification of SiO_2 gas. These particles can provide a certain level of protection to the carbon fiber[33]. However, as the temperature goes higher than 1 700 ℃, SiC undergoes active oxidation, leading to the loss of carbon fiber protection. The direct exposure of SiC to the air causes the generation of gaseous SiO and CO. SiO reacts with O_2, forming molten SiO_2 through pore transport, while CO aggregates to form bubbles, and the rupture process accelerates the ablation[34].

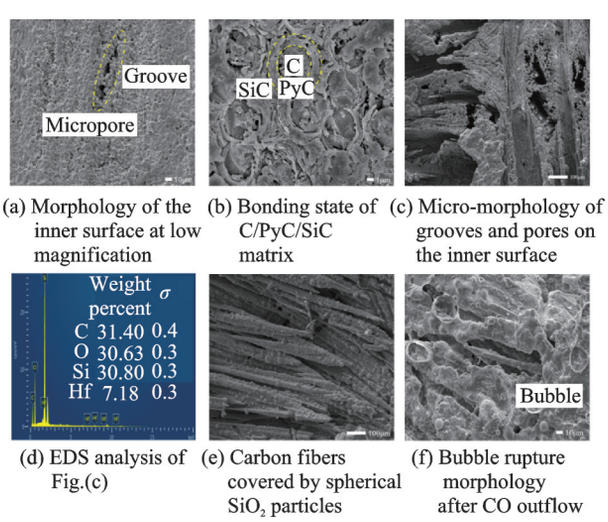

(a) Morphology of the inner surface at low magnification (b) Bonding state of C/PyC/SiC matrix (c) Micro-morphology of grooves and pores on the inner surface

(d) EDS analysis of Fig.(c) (e) Carbon fibers covered by spherical SiO_2 particles (f) Bubble rupture morphology after CO outflow

Fig.7 Different morphologies of the inner surface after removal of the white deposition layer at WT2

In the arc-heated wind tunnel environment, the airflow is parallel to the surface of the sample, resulting in a high velocity of the main airflow. Figs.8(a, b) illustrate significant damage to SiC matrix and carbon fiber at the front end of the leading edge due to mechanical erosion caused by airflow. Various morphologies, such as carbon fiber breakage, fiber pull-out, and filamentous SiO_2 can be observed. The combined analysis of Figs.8(c,d) reveal that the surface is covered with molten SiO_2. Some of the generated SiO_2 is carried away by the high-speed airflow, exposing the carbon fiber, while the remaining SiO_2 attaches to the surface, forming a microcrystal stack structure. This structure enhances thermal resistance and fills pores and cracks at high temperature, and consequently effectively protects the inner layer, then improves the ablation resistance.

The design of V-shaped passivated front edge

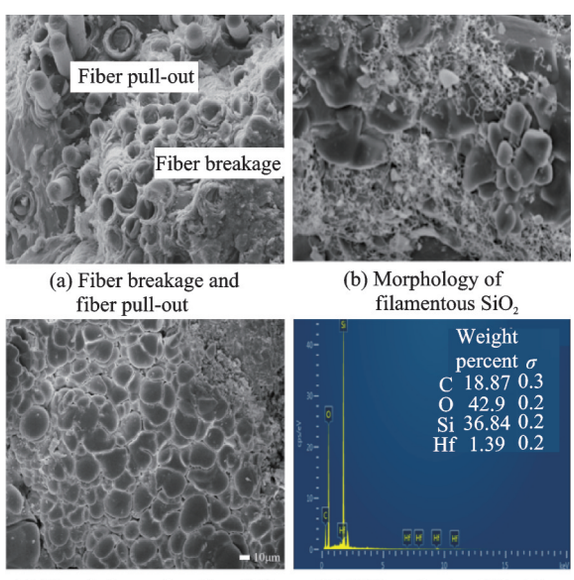

(a) Fiber breakage and fiber pull-out (b) Morphology of filamentous SiO_2

(c) Morphology of molten SiO_2 (d) EDS analysis of Fig.(c)

Fig.8 The front-end ablation morphology of the sample

ensures a smooth surface without forming any sharp angles on the sample. By optimizing the airflow direction and speed, its impact and vibration on the structure are reduced, resulting in low resistance and improved material utilization efficiency. Additionally, it isolates the high-temperature area from the low-temperature area, minimizing heat transfer and relieving thermal stress to protect the integrity of the leading edge and rear-end materials. The most severe ablation occurs near the symmetry center of the leading edge, specifically at WT1 stagnation point. From the sample placement position, it can be seen that the airflow in the center position is parallel to the surface.

After ablation, the microscopic morphology analysis of the central area shows a ladder-like structure. Interlayer erosion is observed near WT1 stagnation point (Fig.9(a)) along with a thin shell structure (Fig.9(b)). Additionally, different fiber orientations exhibit varying degrees of ablation (Fig.9(c)), with distinct annular pores prominently visible in the *Z* direction (Fig.9(d)), and the ablated carbon fibers display a "bamboo shoot-like" structure. The oxidation of needle-punched fibers triggers the peeling off of carbon fibers from SiC matrix, forming thin shell structure. The presence of inter-bundle holes creates the channel for oxygen diffusion, further exacerbating the non-uniform ablation. The "shoot-like" morphology predominantly

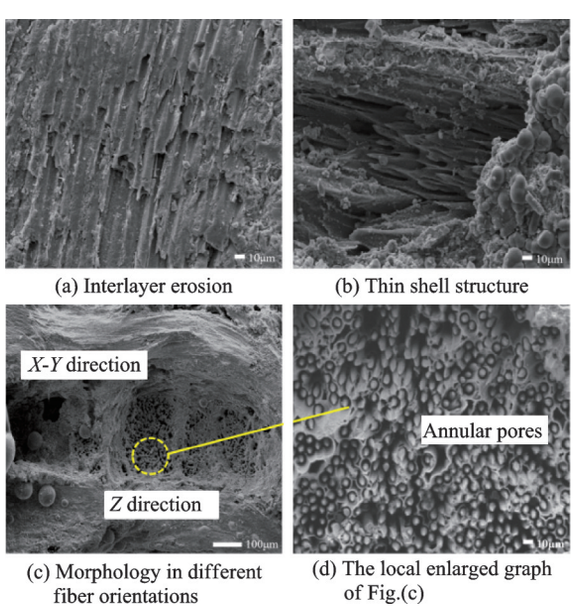

Fig.9 Ablation morphologies near the stagnation point of WT1

occurs due to the high failure strain of SiC matrix compared to the carbon fiber. Under a certain stress level, the matrix cracks first, allowing oxygen to diffuse through microcracks, which oxidize the interface layer and carbon fiber. Consequently, the ablation rate of SiC matrix exceeds that of the carbon fiber[35]. Additionally, the diffusion process of gaseous products (generated in the thermochemical reaction) leads to a concentration gradient, leading to different oxidation times for the front and rear ends of the carbon fiber, which forms "bamboo shoot-like" morphology.

From Fig.3, the transfer of heat is limited during the climb and acceleration stages of aircraft operation, resulting in a substantial temperature gradient at the leading edge. The temperature gradient can stimulate structural thermal stress and deformation. As a result, variations in temperature occur at three stagnation points. As the heat flow density increases to 8 MW/m^2, the surface temperature at the three stagnation points gradually stabilize. At the WT1 stagnation point, the destruction of the formed oxide layer under high heat flux density and high stagnation point pressure make the temperature jump. The immediate burning of the exposed carbon fiber increases temperature. The temperature declines due to the absorption of a significant amount of heat by SiO_2 molten layer through the endothermic process and phase change of SiO_2 in a high-temperature environment. Eventually, the temperature reaches a new steady state. After the ablation test, the temperature continues to rise because of high-temperature and high-pressure state of test chamber without intense airflow flushing, which gradually increases the temperature of the sample. The overall variation in temperature is almost similar at the stagnation point, while WT3 shows a slightly lower temperature. It may be due to uneven heating or airflow disturbance in the arc-heated wind tunnel, which generates an asymmetric distribution of the flow field at WT3. As a result, low heat accumulation reduces temperature.

Interlayer ablation primarily refers to the flaking caused by the thermal stress. The combined impact of the aerodynamic force generated by high-speed airflow and high-temperature and shear force enables *X-Y* carbon fibers more prone to denudation. The oxi-

dation is not uniform, and the anisotropy of C/SiC composites leads to different rates of carbon fiber ablation along XY and Z directions. As the carbon fiber is exposed to airflow, it undergoes oxidation and develops holes, facilitating the diffusion of oxygen. On the other hand, the X-Y alignment of carbon fibers perpendicular to the direction of heat flow (Fig.9(c)), effectively blocks heat from passing through the material and reduces the ablation rate. Additionally, the rapid combustion occurs parallel to the airflow. As the speed of airflow increases, the aerodynamic ablation accelerates the removal of the surface, causing a wide and deep ablation pit.

2.3 Ablation mechanisms

According to standard Gibbs free energy change analysis, the following reactions occur during the entire ablation process

$$HfC+2O_2(g)=HfO_2+CO_2(g) \quad (3)$$

$$HfC+\frac{3}{2}O_2(g)=HfO_2+CO(g) \quad (4)$$

$$SiC+O_2(g)=SiO(g)+CO(g) \quad (5)$$

$$SiC+\frac{3}{2}O_2(g)=SiO(g)+CO_2(g) \quad (6)$$

$$\frac{2}{3}SiC+O_2(g)=\frac{2}{3}SiO_2+\frac{2}{3}CO(g) \quad (7)$$

$$SiC+2O_2(g)=SiO_2+CO_2(g) \quad (8)$$

$$2C+O_2(g)=2CO(g) \quad (9)$$

$$C+O_2(g)=CO_2(g) \quad (10)$$

$$SiO_2+HfO_2=HfSiO_4 \quad (11)$$

The microscopic morphology analysis after ablation shows that the sample mainly experiences chemical erosion and mechanical erosion in the arc-heated wind tunnel environment. Fig.10 illustrates the ablation mechanism of the sample. During the test, various processes, such as hot gas diffusion, mechanical erosion, and thermal radiation, take place. Along with the influence of multi-phase coupling, the ablation retreat and thermal decomposition of the material surface are caused. Additionally, the internal structure of the material underwent changes due to pyrolysis gas diffusion and heat conduction[36-37]. As the temperature and heat flux density increase during the ablation process of the HfC-coated C/SiC composite samples, the oxidation occurs at the outer HfC coating first (Eqs.(3, 4)). It forms a protective liquid HfO_2 film against ablation. However, a portion of HfO_2 film is carried away due to airflow. In addition, the porous nature of HfO_2 oxide facilitates oxygen to the internal C/SiC composites. Then the oxidation reaction of Eq.(5) occurs. The gaseous SiO and CO accelerate the ablation process. With increasing heat flux density and temperature, dense oxide layers of HfO_2 and SiO_2 appear (Fig.6), which partially obstruct the diffusion of oxygen and slow down the oxidation process of the carbon fiber. Furthermore, a minimal amount of $HfSiO_4$ forms according to Eq.(11)[38]. SiO_2 generated through passive oxidation can possess excellent anti-oxidation capabilities at temperature below 1 850 ℃[15]. Reactions (Eqs.(6—10)) occur during the ablation process, resulting in liquid SiO_2, which leads to the appearance of flow and solid particles on the surface. The white oxide layer consisting of HfO_2 and SiO_2 is peeled off. The presence of a temperature gradient accelerates the ablation of SiC matrix and carbon fiber. HfC coating reduces the oxidation reaction and exhibits good ablation resistance.

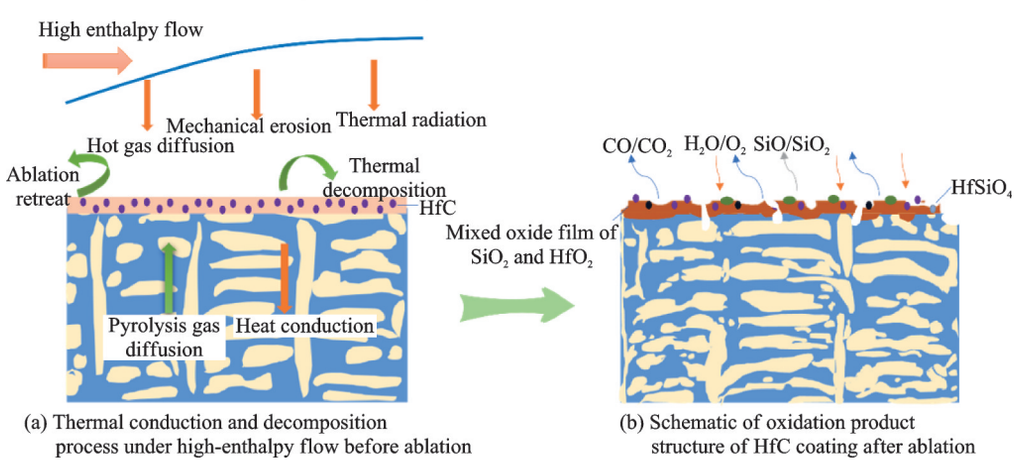

(a) Thermal conduction and decomposition process under high-enthalpy flow before ablation

(b) Schematic of oxidation product structure of HfC coating after ablation

Fig.10 Ablation mechanism of HfC coated 2.5D needled C/SiC composites

3 Conclusions

The HfC-coated 2.5D needle-punched composites is tested in an arc-heated wind tunnel to simulate re-entry conditions. By analyzing the macroscopic morphology and microstructure evolution, the ablation performance of the aircraft under a high-enthalpy flow environment is investigated to analyze ablation mechanisms through experiments and theoretical models. After long-term ablation, the sample's profile remains intact with minimal surface layer ablation and no significant internal damage. The total mass ablation rate is measured to be 0.074 45 g/s, the average linear ablation rate in the thickness direction is −0.067 5 μm/s, and the average linear ablation rate in the length direction is 13.907 μm/s. The ablation of C/SiC composite primarily occurs through chemical erosion and mechanical ablation. The synergistic effect of the outer oxide layer and inner dense layer provides excellent ablation resistance and antioxidant properties. Through the ablation test and analysis of test results, along with the analysis of the ablation mechanism, it is clearly demonstrated that the plasma-sprayed HfC coating exhibits good antioxidant and ablation properties. This coating effectively addresses the ablation challenges encountered by C/SiC composites at temperature exceeding 1 700 ℃. This study provides essential data for the development of thermal protection materials and the evaluation of structural thermal performance in hypersonic aircraft.

References

[1] PADTURE N. Advanced structural ceramics in aerospace propulsion[J]. Nature Materials, 2016, 15(8): 804-809.

[2] LUO L, WANG Y, LIU L, et al. Carbon fiber reinforced silicon carbide composite-based sharp leading edges in high enthalpy plasma flows[J]. Composites Part B: Engineering, 2018, 135: 35-42.

[3] VINH T L, NGOC S H, NAM S G. Advanced sandwich structures for thermal protection systems in hypersonic vehicles: A review[J]. Composites Part B: Engineering, 2021, 226: 109301.

[4] YANG L, JING L, ZHANG J, et al. Excellent ablation resistance and reusability of silicon carbide fiber reinforced silicon carbide composite in dissociated air plasmas[J]. Journal of the European Ceramic Society, 2023, 43(5): 2275-2281.

[5] PI H L, SONG F, WANG H D, et al. Influence of copper contamination on ablation damage of C/SiC composites under simulated thermal environment of arc heater[J]. Ceramics International, 2021, 47(15): 22016-22024.

[6] WU D, WANG Y, SHANG L, et al. Thermo-mechanical properties of C/SiC composite structure under extremely high temperature environment up to 1 500 ℃[J]. Composites Part B: Engineering, 2016, 90: 424-431.

[7] TRIANTOU K, MERGIA K, FLOREZ S, et al. Thermo-mechanical performance of an ablative/ceramic composite hybrid thermal protection structure for re-entry applications[J]. Composites Part B: Engineering, 2015, 82: 159-165.

[8] YANG L, JING L, ZHANG J, et al. New insights on the ablation mechanism of silicon carbide in dissociated air plasmas[J]. Aerospace Science and Technology, 2022, 129: 107863.

[9] SONG C, YE F, CHENG L, et al. Long-term ceramic matrix composite for aeroengine[J]. Aerospace Science and Technology, 2022, 11: 1343-1374.

[10] WANG X, GAO X, ZHANG Z, et al. Advances in modifications and high-temperature applications of silicon carbide ceramic matrix composites in aerospace: A focused review[J]. Journal of the European Ceramic Society, 2021, 41: 4671-4688.

[11] DUAN N, SHI X, WANG J, et al. Multilayer-structured carbon fiber fabric/graphene oxide/Fe_3O_4/epoxy composite for highly efficient mechanical and electromagnetic interference shielding[J]. Applied Surface Science, 2023, 613: 156038.

[12] LUO L, WANG Y, LIU L, et al. Ablation behavior of C/SiC composites in plasma wind tunnel[J]. Carbon, 2016, 103: 73-83.

[13] SAMMAIAH P, MANIVANNAN M, RAKESH G. Review article on oxidation protective UHTC coatings for C/C and C/SiC composites[C]//Proceedings of International Conference on Research in Sciences, Engineering & Technology. Warangal, India: AIP Conference Proceedings, 2022, 2418(1): 050007.

[14] POVOLNY S J, SEIDEL G D, TALLON C. Investigating the mechanical behavior of multiscale porous ultra-high temperature ceramics using a quasi-static material point method[J]. Mechanics of Advanced Materials and Structures, 2021, 160(3): 103976.

[15] NI D, CHENG Y, ZHANG J, et al. Advances in ultra-high temperature ceramics, composites, and coat-

ings[J]. Journal of Advanced Ceramics, 2022, 11(1): 1-56.

[16] JIN X, FAN X, LU C, et al. Advances in oxidation and ablation resistance of high and ultra-high temperature ceramics modified or coated carbon/carbon composites[J]. Journal of the European Ceramic Society, 2018, 38(1): 1-28.

[17] KUMAR C V, KANDASUBRAMANIAN B. Advances in ablative composites of carbon based materials: A review[J]. Industrial & Engineering Chemistry Research, 2019, 58: 22663-22701.

[18] YANG X, WEI L, SONG W, et al. Ablative property of ZrC-SiC multilayer coating for PIP-C/SiC composites under oxy-acetylene torch[J]. Ceramics International, 2012, 38(4): 2893-2897.

[19] GENG L, CHENG S, GUO C, et al. Ablation behavior of C/SiC with YSZ and ZrB_2 coatings under high-energy laser irradiation[J]. Ceramics International, 2023, 49(2): 1700-1709.

[20] YAO M, GOU Y, HE Y. Research progress on high-temperature protection coatings[J]. China Powder Science and Technology, 2005, 11(3): 32-43.

[21] REN J, FENG E, ZHANG Y, et al. Microstructure and anti-ablation performance of HfC-TaC and HfC-ZrC coatings synthesized by CVD on C/C composites[J]. Ceramics International, 2020, 46(8): 10147-10158.

[22] BINNER J, PORTER M, BAKER B, et al. Selection, processing, properties and applications of ultra-high temperature ceramic matrix composites, UHTCMCs—A review[J]. International Materials Reviews, 2020, 65(7): 389-444.

[23] YANG Y, ZHAO C, GONG Q, et al. Ablation resistance under different heat fluxes of HfC-ZrC-SiC multiphase coating prepared by supersonic atmospheric plasma spraying for C/C composites[J]. Journal of the Korean Ceramic Society, 2020, 57: 152-160.

[24] PENG L, TAN Q, LIU L, et al. Research progress on preparation technology of spherical powder[J]. China Powder Science and Technology, 2024, 30(3): 12-27.

[25] SUN H, JIA J, YANG J, et al. Preparation of nanostructured MoO_3-Bi_2O_3 composite powder for plasma spraying[J]. China Powder Science and Technology, 2021, 27(6): 29-36.

[26] SUN H, ZHANG J, DIAN D, et al. Research on nano-structured Al_2O_3-TiO_2-SiO_2-SiC feedstock for plasma spraying[J]. China Powder Science and Technology, 2008, 14(5): 41-44.

[27] YOO H I, KIM H S, HONG B G, et al. Hafnium carbide protective layer coatings on carbon/carbon composites deposited with a vacuum plasma spray coating method[J]. Journal of the European Ceramic Society, 2016, 36(7): 1581-1587.

[28] LI Y, WANG J, ZHANG J, et al. Interfacial heat transfer characteristics and thermal expansion behavior of heterostructure materials in arc-heated wind tunnel[J]. Mechanics of Advanced Materials and Structures, 2023, 176: 104488.

[29] KONG Y, ZHANG J, YUE M, et al. Investigation of the bulging mechanism of C/SiC coating through in situ optical observation and numerical simulation[J]. Ceramics International, 2021, 47(14): 20456-20466.

[30] TANG Y, YUE M, FANG X, et al. Evolution of surface droplets and flow patterns on C/SiC during thermal ablation[J]. Journal of the European Ceramic Society, 2019, 39(13): 3566-3574.

[31] KOIDE N, MARUMO T, ARAI Y, et al. Degradation of carbon fiber-reinforced ultra-high-temperature ceramic matrix composites at extremely high temperature using arc-wind tunnel tests[J]. Journal of Materials Science, 2022, 57: 19785-19798.

[32] JU Y, LIU X, WANG Q, et al. Ablation behavior of ultra-high temperature composite ceramic matrix composites[J]. Journal of Inorganic Materials, 2022, 37: 86-92.

[33] LIU Y, XIA Z, MA L, et al. Microstructure and ablation mechanism of C/C-ZrC-SiC composite in the solid scramjet plumes environment[J]. Materials Characterization, 2023, 198: 112754.

[34] CHENG S, DUAN L, GENG L, et al. Ablation behavior of C/SiC composite chamber in a kerosene/oxygen combustion environment[J]. Journal of the Chinese Ceramic Society, 2018, 46(12): 1685-1693.

[35] WANG L, WANG K, ZHANG X, et al. Effect of high temperature oxidation and particle erosion on the performance of C/C-SiC composites materials[J]. Hangkong Cailiao Xuebao/Journal of Aeronautical Materials, 2022, 42(4): 75-82.

[36] PAN Weizhen, YI Fajun. An identification method for thermal properties of ablative thermal protection materials[J]. Journal of Nanjing University of Aeronautics & Astronautics, 2022, 54(S): 100-108. (in Chinese)

[37] HAO Weu, LI Ming, WANG Yingchun. Characteristics of defects and its ultrasonic defection in large curvature composite[J]. Journal of Nanjing University of Aeronautics & Astronautics, 2017, 49(S1): 56-61. (in Chinese)

[38] JIAO X, TAN Q, HE Q, et al. Cyclic ablation behav-

ior of mullite-modified C/C-HfC-SiC composites under an oxyacetylene flame at about 2 400 ℃[J]. Journal of the European Ceramic Society, 2023, 43(10): 4309-4321.

Acknowledgements This work was financially supported by the National Key R&D Program of China (No.2022YFB3-401900), the National Natural Science Foundation of China (No.U21A20134), and the Shandong Provincial Natural Science Foundation (Excellent Young Fund, No.ZR2022YQ48).

Authors Ms. **ZHANG Ziyi** received the B.S. degree in engineering from Harbin Institute of Technology. She is currently a graduate candidate at School of Mechanical Engineering, Shandong University. Her research interests focus on ceramic matrix composites.

Prof. **SHI Zhenyu** received the B.S. and Ph.D. degrees in mechanical engineering from Shandong University, Jinan, China, in 2006 and 2011, respectively. From 2012 to 2014, she was a postdoctoral research fellow in the School of Material Science and Engineering, Shandong University, Jinan, China. From 2012 to 2023, she worked at School of Mechanical Engineering at Shandong University and served as a professor in the Key Laboratory of High Efficiency and Clean Mechanical Manufacture at Shandong University. Since 2023, she has been working at School of Mechanical Engineering at Hebei University of Technology. Her research has focused on material science and green manufacturing process, which includes composite material preparation, surface modification, high-speed cutting process, surface integrity and environment-friendly processing method.

Author contributions Material preparation, and data collection and analysis were performed by Ms.**ZHANG Ziyi**, Prof. **SHI Zhenyu** and Dr.**WANG Jilai.** The first draft of the manuscript was written by Ms. **ZHANG Ziyi**. Manuscript review and editing were performed by Prof. **NI Jing** and Prof. **ZHANG Chengpeng**. All author scontributed to the study conception and design, and commented on the manuscript draft and approved the submission.

Competing interests The authors declare no competing interests.

(Production Editor: XU Chengting)

用于高超声速飞行条件下航天发动机的HfC涂层2.5D针刺复合材料烧蚀过程研究

张子怡[1,2]，史振宇[3]，倪　敬[4]，王继来[1,2]，张成鹏[1,2]

(1.山东大学高效洁净机械制造教育部重点实验室，济南 250061，中国；2.山东大学机械工程学院，济南 250061，中国；3.河北工业大学机械工程学院电工装备可靠性与智能化国家重点实验室，天津 300130，中国；4.杭州电子科技大学机械工程学院，杭州 310012，中国)

摘要：航天发动机的工作环境极为严苛，温度超过1 700 ℃，并伴随热耦合效应。在这种极端条件下，应用于高超声速飞行器的材料面临烧蚀风险，可能导致灾难性事故。由于HfC具有优异的高温稳定性和抗烧蚀性能，并且其热膨胀系数与C/SiC复合材料相匹配，因此成为理想的材料选择。本文采用等离子喷涂工艺制备了HfC涂层的2.5D针刺C/SiC复合材料，并利用高焓电弧加热风洞模拟了飞行器在8马赫速度和32 km高度下的再入环境。随后，对这些等离子喷涂的HfC涂层2.5D针刺C/SiC复合材料进行了长期动态测试，重点研究了其性能表现。特别是在热评估烧蚀实验后，复合材料的整体结构和轮廓得以保持；其总质量烧蚀速率为0.074 45 g/s，厚度方向的平均线性烧蚀速率为－0.067 5 μm/s，长度方向的平均线性烧蚀速率为13.907 μm/s。结果验证了等离子喷涂HfC涂层的卓越抗氧化和抗烧蚀性能。此外，还对C/SiC复合材料的微观结构和烧蚀机理进行了深入研究。本研究将为热防护材料的开发和结构热性能的评估提供重要指导。

关键词：2.5D针刺C/SiC复合材料；烧蚀机理；电弧加热风洞实验；高焓流